LASER VELOCIMETRY IN HIGHLY THREE-DIMENSIONAL AND VORTICAL FLOWS

Charles J. Novak, Charles R. Huie, and Kenneth C. Cornelius
Lockheed-Georgia Co.
Marietta, Georgia

SUMMARY

The need for experimentally determined 3-D velocity information is crucial to the understanding of highly 3-dimensional and vortical flow fields. In addition to gaining an understanding of the physics of flow fields, a correlation of velocity data is needed for advanced computational modelling. A double pass method for acquiring 3-D flow field information using a 2-D laser velocimeter (LV) is described. The design and implementation of a 3-D LV with expanded capabilities to acquire real-time 3-D flow field information are also described. Finally, the use of such an instrument in a wind tunnel study of a generic fighter configuration is described. The results of the wind tunnel study highlight the complexities of 3-D flow fields, particularly when the vortex behavior is examined over a range of angles of attack.

INTRODUCTION

Since its conception by Yeh and Cummins (ref. 1) of Columbia University in 1964, the laser velocimeter (LV) has proved itself to be a most useful non-intrusive flow field velocity measuring instrument. Early versions of the instrument were limited to single direction velocity measurements and soon evolved to 2-D with reverse flow measurement capability. Yanta, in a recent paper (ref. 2), has described the LV's usefulness in the field of wind tunnel testing. Lockheed-Georgia Co. started LV research in 1968 and has had a continuing role in instrumentation development since then. Examples of the type of flow field measurements that have been acquired to date are shown in figures 1 and 2. These 2-D flow field vector plots have been the result of substantial efforts in LV research and application and have led to a better understanding of the physics of unpowered and powered flow fields.

Recent efforts in the analysis of three-dimensional (3-D) flow fields by the technique of computational fluid dynamics (CFD) have driven the need to develop fully 3-D measurement capabilities. The goal of Lockheed's research has been the development of a 3-D instrument for measurements in highly three-dimensional and vortical flow fields.

INTERIM TECHNIQUE

During the period of 3-D LV development, the need for 3-D flow field information became so great that a double-pass, or as to be labeled further, a 2 x 2-D method of 3-D velocity measurement was developed. This method is comparatively low cost based on instrumentation requirements; however, an attendant two-fold increase in test time may make it unsuitable for many wind tunnel tests.

The use of the 2 x 2-D method is relatively straightforward and involves the use of a 2-D LV. Two sets of measurements are made with pre-determined fringe orientations with respect to the wind tunnel coordinate system. Orientation of the first and second measurement fringe geometries (second set of measurements made later in time with respect to the first set) along with tunnel coordinates is shown in figure 3. These two sets of measurements result in 2-D velocity information in the plane H_1 -R_1 and H_2 -R_2 . Note that in this figure the vertical fringes are parallel in both measurement orientations ($R_1 = R_2$). The desired end result, the on-axis velocity component, W, in the z direction, is found by subsequent post-processing of the two data sets.

Method Description

Data reduction is done off-line and is based on a formulation similar to that of 3-D hot wire anemometry. This formulation is the heart of the method and is left general for the sake of completeness. First, consider direction cosines with respect to the tunnel coordinate system and the instantaneous fringe velocities; that is, a_1, a_2, b_1, b_2, c_1, c_2, and H_1, R_1. Conversely the same may be done with respect to the second set of measurements so that a_3, a_4, b_3, b_4, c_3, c_4 are used as direction cosines for the two perpendicular fringe velocities H_2, R_2. Finally, based on the determined direction cosines, each measured velocity component (H_1 - R_2) may be expressed as a combination of the tunnel velocities and direction cosines. This results in:

$$a_1 U + b_1 V + c_1 W = H_1 \tag{1a}$$

$$a_2 U + b_2 V + c_2 W = R_1 \tag{1b}$$

$$a_3 U + b_3 V + c_3 W = H_2 \tag{1c}$$

$$a_4 U + b_4 V + c_4 W = R_2 \tag{1d}$$

yielding an overspecified set of equations which may be solved for the instantaneous tunnel velocities U, V, and W using an appropriate least-squares optimization of simultaneously solved equations.

Now, it is convenient to differentiate between mean and instantaneous velocities. This is done by assuming a mean velocity $\bar{U}$, and the departure from that mean as the velocity u'. Using that premise, equation 1a becomes:

$$a_1 (\bar{U}+u') + b_1 (\bar{V}+v') + c_1 (\bar{W}+w') = (\bar{H}_1 + h_1') \tag{2}$$

The same may be performed for R_1, H_2, and R_2, but is not shown here for brevity's sake. Further, if equation 2 is squared and then time averaged the end result is:

$$a_1^2 \bar{u}^2 + b_1^2 \bar{v}^2 + c_1^2 \bar{w}^2 + a_1 b_1 \overline{uv} + a_1 c_1 \overline{uw} + b_1 c_1 \overline{vw} = \bar{h}_1^2 \tag{3}$$

Once again similiar expressions may be derived for $\bar{r}_1^2$, $\bar{h}_2^2$, and $\bar{r}_2^2$. Note that equation 3 contains the six principal Reynolds stresses as unknowns. Compiling these results yields 4 equations and 3 unknowns in the mean velocities and 4 equations and 6 unknowns in the time-averaged fluctuating or turbulence quantities. Clearly the experimentalist faces a dilemma in solving for the turbulence quantities in the flow field. He may either choose to use only mean velocities or use appropriate fringe orientations such that terms drop out. However, if 2-D instrumentation capabilities are examined and utilized fully, the measurement of H_1, R_1 and H_2, R_2

may be made such that the fluctuating cross products $\overline{h_1 r_1}$ and $\overline{h_2 r_2}$ are formed. This requirement of coincidence is needed to close the set of equations containing the six Reynolds stresses. Then, proceeding as before the expression for $\overline{h_1 r_1}$ becomes:

$$\overline{h_1 r_1} = a_1 a_2 \bar{u}^2 + b_1 b_2 \bar{v}^2 + c_1 c_2 \bar{w}^2 + (a_1 b_2 + a_2 b_1)\overline{uv} + (a_1 c_2 + a_2 c_1)\overline{uw} + (b_1 c_2 + b_2 c_1)\overline{vw} \quad (4)$$

Similarly, an expression for $\overline{h_2 r_2}$ may be written. These two equations are then combined with the four previously derived equations, yielding 6 linear equations and 6 unknowns, all of which may be solved easily using a matrix inversion routine. The end result of this scheme is full 3-D flow field information to the first statistical moment.

2 x 2-D Method Usage

Usage of the method should be based upon data requirements and with these needs defined, fringe-tunnel geometries must be chosen with some discretion. If those details are ignored, matrix singularities may occur making the desired quantities unresolvable. Therefore, a prior knowledge of matrix behavior is desirable since some quantities, such as $\overline{uw}$ and $\bar{w}^2$, may require pitch and roll in addition to yawing of the fringe systems with respect to the tunnel coordinates.

Errors in the method not only reflect uncertainties in the LV electronics but also in fringe angles and repositioning. As noted in figure 3, the redundancy in the V component ($R_1 = R_2$) is not without purpose. Specifically, data quality is enhanced dramatically if profile matching is done with either $\bar{V}$ or $\bar{v}^2$. Each of the corresponding sets of measurements is interpolated for any spatial offsets and their differences in position are averaged. Further, uncertainties also arise from inaccuracies in determining fringe angles with respect to the tunnel coordinate system. Reduction of these uncertainties is discussed fully by Orloff and Snyder (ref. 3) and the same principles were employed in the present work. Also as in their work, adoption of a rotating calibration device aided in reducing errors considerably during implementation of the 2 x 2-D method.

Wind Tunnel Tests Using 2 x 2-D Method

The usefulness of this technique is illustrated in two experiments where 3-D LV information was provided through the 2 x 2-D methodology. The first experiment was designed to provide correlation data for 3-D boundary layer code development using advanced turbulence modelling. The wind tunnel model used was a low-aspect-ratio, highly swept fighter type wing on which upper and lower surface velocity measurements were made. Shown in figure 4 are the boundary layer profiles for both the chordwise and spanwise velocity components at 60% span on the lower surface. Shown in figure 5 is a contour map, in the survey region on the lower surface, of the dimensionless turbulence anisotropy parameter T. For isotropic flow, the value of T, as constructed from mean flow gradients and $\overline{uv}$ and $\overline{vw}$ shear stresses, tends to 0.5. Physically, it reflects the relative rate at which the chordwise and spanwise velocity gradients develop. Values of T tending towards zero represent turbulence that is predominantly strained in W or the spanwise direction and for values greater than one, straining is dominant in the chordwise direction.

A second experiment specifically designed to aid development of a coupled 3-D boundary layer and Euler code was successfully carried out using the 2 x 2-D method. In this experiment the wind tunnel model consisted of an aft-fuselage, representative of that for a modern transport aircraft. LV velocity surveys were conducted in both the open separation region and the near wake. Figure 6a shows the mean crossflow velocity profiles at a particular cross section station on the model and depicts the experimental line of crossflow reversal. Further, the presence of the trailing vortex can be seen in the streamwise velocity contours, as can be the fuselage and wing wakes, figure 6b.

The merits of the 2 x 2-D method are demonstrated in the types of data that become available with its employment in wind tunnel testing. However, due to inaccuracies and the time requirements involved with its use, a fully 3-D instrument would eclipse its usefulness in a typical production basis.

3-D LV DEVELOPMENT

Instrument Definition

At the conceptual stage of the 3-D LV development program substantial goundwork was laid with electronics/signal requirements. Previous 2-D experience showed that a simple one channel expansion to the current design would provide excellent signal handling capabilities. Therefore, the electronics used was based upon the single cycle validation circuitry and dual counter approach used previously on the 2-D instrument. From a design standpoint, important electronics/signal processing constraints were firmly established in the prior use of the 2-D burst-type detector electronics. This was the foundation for the 3-D LV development.

Velocity range and resolution are probably the most important of all constraints; however, optical system geometry, which defines accessibility to the flow field, is also a consideration from the practical standpoint. In addition to mean velocity measurement, turbulence intensities and other higher statistical moments about the mean are also needed. Additionally, in the realm of unsteady aerodynamics, temporal data may be required, either as conditionally sampled data or as spectral information about the flow field in question. Lastly, the 3-D instrument must be usable on a production testing basis. This includes stable alignment and substantial data rates that are comparable with existing 2-D instrumentation.

Optical System Choices

For wind tunnel testing purposes the logical choice for a light source is the Argon-Ion laser. This laser commonly used for wind tunnel testing has principal emission lines at wavelengths of 488.0 nm (blue) and 514.5 nm (green), each of which contains approximately 30% of the total power output. Additional emission lines located at 476.5 nm (deep blue) and 496.5 nm (blue-green) contain 10% each of the total power. Thus, the developer is given the choice of 4 emission lines to utilize, typically only two (488.0 and 514.5 nm.) or three (488.0,514.5 and 476.5 nm.) of which are used for three-component velocity measurements. Regardless of wavelength, the on-axis velocity component must be measured with a separate set of fringes or indirectly through a non-orthogonal technique.

In addition to wavelength selection and fringe orthogonality or non-orthogonality, a choice between frequency domain or velocity domain processing of the Doppler signal may be of particular advantage for W component extraction. The

choices to be considered are presented in figure 7 and are based upon known techniques in arriving at the much sought after third component. Relative merits of each configuration must be weighed with respect to the type of use the instrument will see, and an indepth study of each is warranted.

Optical Selection and Design

The construction of the existing wind tunnels at the Lockheed-Georgia Company and the lack of windows in the floors and ceilings make orthogonal fringe orientation impracticable. Further, previous experience has shown that a 3-D orthogonal system would almost always have a set of laser beams oriented perpendicular to the model's surface. This would represent serious glare problems and would render the system unusable in near-wall measurements. For these reasons the orthogonal fringe systems were removed from the selection process. As seen in figure 7, the remaining choices are from the non- orthogonal fringe category and are comprised of either a two or a three-color optical configuration. However, prior to optical and electronics fabrication a comparison of the operational aspects of each of these two types of optical configurations, as shown in figure 8, was performed.

Velocity range and resolution may be easily understood if the concept of effective fringes is introduced. As a means of understanding effective fringes, consider two non-orthogonal fringe systems propagating at 40 MHz and 60 MHz respectively and separated by an angle 2k. This wavefront geometry is shown in figure 9 and may either be formed by a single wavelength or by two wavelengths such as the two and three-color systems would produce. Analyzing the expected photo-multiplier tube (PMT) signals it can be seen that they will contain both a frequency component from the carrier (40 and 60 MHz) and one from the velocity of the media itself. This is seen clearly if the conventional expression for velocity is applied for each separate fringe system such that:

$$H_1 = \frac{\lambda}{2 \sin \theta/2} \left(f_{media} - f_{shift_1}\right) \quad f_{shift} = 40 \text{ MHz} \qquad (5)$$

$$H_2 = \frac{\lambda}{2 \sin \theta/2} \left(f_{media} - f_{shift} \right)_2 \quad f_{shift} = 60 \text{ Mhz} \qquad (6)$$

where λ and θ are the respective wavelength and beam angles that contribute to the formation of the fringes. Note that the first term in equations 5 and 6 corresponds to the fringe spacing. From the 2 x 2-D method presented earlier it can be shown that the transverse, or on-axis velocity component, W, based only on yaw with respect to the tunnel coordinate system, is simply:

$$W = \frac{H_1 - H_2}{2 \sin k} \qquad (7)$$

and k is the half angle between the fringe systems. Substituting equations 5 and 6 into equation 7 yields

$$W = \frac{\lambda}{4 \sin k \sin(\theta/2)} (\Delta f_{media} - \Delta f_{shift}) \quad \Delta f_{shift} = 20 \text{ Mhz} \qquad (8)$$

Note that this result, equation 8, bears resemblance to the original fringe spacing equations 5 and 6. Therefore, it is possible to think of the first term in equation 8 as the effective fringe spacing in the transverse direction and the second term as the associated frequency corresponding to the fringe crossing in units of inverse time. This concept of effective fringes (also shown graphically in figure 9 as the dashed lines perpendicular to the on-axis direction) is the backbone of the 3-D LV in non-orthogonal fringe systems and is made use of in velocity range and resolution comparisons.

Using this concept of effective fringes, a comparison of frequency and velocity domain processing (sometimes called pre- and post-processing) can be made. Frequency domain processing is carried out by heterodyning the two PMT signals containing the W component such that the U component is essentially removed from the signal leaving only that corresponding to W. From a practical standpoint this may be achieved by employing double balanced diode mixers. These mixers, also used to heterodyne the Bragg cell shift to a manageable range, operate on the basis that the local oscillator (LO) side is maintained at a constant amplitude of + 7dBm. The reference (RF) side power level may be varied from -20dBm, where typical Doppler signals lie, all the way up to 0dBm. Noise levels increase when these input specifications are not met. So when using the circuits in actual testing, significant amplification is needed on the LO input side, as is seen in figure 10, to raise the signal to design specification levels. This represents the major drawback to frequency domain processing in the non-orthogonal fringe systems. Not apparent from figures 9 and 10 is an operational benefit that ensures against the likelihood of two particles in separate regions of the measurement volume being seen and processed as one particle. The heterodyning of the two signals, such that a W signal is formed, also eliminates the possibility of this situation occurring unless they enter and leave the fringe systems at the same point in time.

In comparison with frequency domain processing, velocity domain processing of signals eliminates the need for additional filters, amplifiers and mixers in the system. Instead of using effective fringes, the individual velocities from the non-orthogonal fringes are computed in a traditional 2-D manner and later combined discretely sample by sample (three-channel coincidence required during acquisition). Typically, higher uncertainties are present at this level of processing since uncertainties are additive, and unlike in frequency domain processing, amplitude restrictions do not exist. This may in turn help the signal-to-noise ratio (SNR) of the instrument in low SNR regions in the flow field.

Velocity Range and Resolution Determined

As an aid in comparing the two- and three-color 3-D LV optics configurations, an analytical model was developed to determine velocity range and resolution for a given set of input parameters. These included laser beam diameter, counter resolution and bandwidth, beam angles and fringe angles. Outputs of the model were effective fringe spacing, velocity range and resolution as well as frequency bandwidth. Using this model for initial comparisons yielded information that led to the selection of the most suitable optics configuration for highly three-dimensional and vortical flow fields.

Examples of the output of this model are shown in figures 11 and 12. Figure 11 is a plot of separation angle versus effective fringe spacing for several beam pair angles. With the existing 2-D beam pair angles (θ) at approximately 3.8 degrees and fringe spacings of 20 μm, it is seen that substantial separation angles are needed to give effective fringe spacings of 20 μm to 30 μm. Once an effective fringe spacing is determined from figure 11 the user can proceed to figure 12 where velocity range and resolution are determined. To determine velocity range, the minimum beam diameter (DE (mm)) is examined at the operating bandwidth of the electronics and the upper velocity limit is noted at this intersection on the horizontal velocity axis. Similarly, resolution is obtained for a given bandwidth and effective fringe spacing (D_f (μm)) by noting the intersection of the two curves on the horizontal axis. In addition to range and resolution, the bandwidth for a particular velocity range is also available through the use of figure 12. This is done simply by noting the angle of the focused laser beam pairs (θ) that applies and using that curve to determine the value of frequency bandwidth for a given velocity.

Using these charts to compare 3-D LV optics packages it was possible to determine performance prior to fabrication. Based on range and resolution requirements, typical of what is needed for vortical flows, the frequency bandwidth for the two-color system was found to overlap from one channel to another. To avoid this, the resolution became unacceptable, since the effective fringe spacing had to be made larger to increase the velocity range. Further complicating the matter, the wide fringe spacing also decreases the number of fringes in the measurement volume making alignment sensitive and valid data signals unavailable. Contrasting the two-color performance, the three-color system separates channels by wavelength (color) and not by bandwidth separation, hence, velocity crosstalk is non-existent for this optics package. For that reason the three-color system is more suitable since its upper velocity limits are dictated by the counter input bandwidth rather than the frequency crosstalk bandwidth. Thus, because velocity range and resolution are decoupled in the three-color system, resolution needs not be sacrified for range when operating in flow fields where the transverse component may vary from zero to more than that of the freestream.

In addition to velocity measurement capabilities, a rather particular advantage of the three-color system in frequency domain processing was discovered during preliminary studies. Shown in figure 13 are block diagrams of the necessary electronics needed to frequency separate and mix signals such that the signal contributing to the W effective fringes may be processed. Note that one less signal split is needed in the three-color pre-processor. From an operational standpoint this gain of 2 in signal strength offsets the lower power levels of the third emission line (476.5 nm) from the Argon-Ion laser.

Based on the comparisons of both performance and operational capabilities, the three-color 3-D LV optics configuration was chosen since its merits far outweighed those of its two-color counterpart. While a two-color optics package was built its use is limited to low-speed flows and flows where the transverse component is small.

THREE-COLOR 3-D LV DESCRIPTION

System fabrication and interfacing consisted of updating an existing 2-D system to 3-D capability. To accomplish this an additional set of receiving and transmitting optics was constructed based on the design used previously in 2-D LV studies. The optics, electronics and positioner are shown in figure 14. Previous experience has shown that rotating regions in the flow field may be particle

deficient. Hence, two 18 watt Argon-Ion lasers, one operating at 476.5 nm and the other multi-line, were used to boost signal-to-noise ratios in sparsely seeded regions in the flow field. The current configuration shown in figure 14 has complete flexibility in that both receiving and transmitting optics may be oriented arbitrarily with respect to the model and the wind tunnel. Similiar to the setup of Yanta (ref. 4) is the large included angle between the non-orthogonal fringes. For the testing to be detailed later, the angle was set at 33 degrees, corresponding to a resolution of 0.3 m/sec and an upper velocity limit near 300 m/sec. This flexibility in optical design is advantageous since it reduces the number of regions in which the laser beams are obscured by either the model or the tunnel structure. Receiving optics are purposely separated to take advantage of the Mie scattering qualities that exist. In addition to optical wavelength separation between the 488.0 nm. and 476.5 nm channels, further insurance against optical filter bleed was provided by frequency separation with the use of Bragg cells operating at different frequencies.

Bench tests were conducted prior to production use of the instrument to insure system repeatability and accuracy. Resolution was verified experimentally through the use of a rotating calibration wheel as described earlier for the 2 x 2-D method. These tests were performed for two different fringe angles and compared with theory. As predicted, resolution in W behaved as the inverse sine of the angle 2k between the non-orthogonal fringes. The results of the bench tests at W=0.0 m/sec are as follows:

2k	ΔW Experiment	ΔW Theory
17.5 deg	.769 m/sec (2.5 fps)	.738 m/sec (2.4 fps)
30.0 deg	.462 m/sec (1.5 fps)	.338 m/sec (1.1 fps)

In addition to use during checkout, the rotating calibration device proved to be invaluable for routine alignment on a day to day basis in determining both fringe spacings and angles. With the operational limits established and verified the instrument was readied for production type testing.

3-D LV SURVEYS OF A GENERIC FIGHTER CONFIGURATION

Testing to date with the instrument has been limited because of its recent placement in service. However, this year's testing has included 3-D velocity surveys of a generic fighter configuration for the purpose of both CFD model development and the understanding of the flow field physics. Shown in figure 15 is the model geometry used for both numerically controlled model fabrication as well as for the CFD grid generation. The tip verticals were removed to facilitate LV testing. The geometry consists of a leading-edge strake sweep of 77 degrees followed by a wing sweep of 56 degrees. Testing was carried out in the Lockheed-Georgia Low Turbulence Wind Tunnel (.05% freestream turbulence) at a freestream velocity of 46 m/sec (150 fps). The corresponding Reynolds number based on centerline chord was 1.25 million. Shown in figure 16 are the model, tunnel and 3-D LV optics. Surveys were made of mean velocity in the Y-Z plane of the model at various X locations and several angles of attack and contained approximately 200 points each.

Data rate in the freestream region of the flow field was approximately 500 valid samples per second, whereas near the vortex core, the rate dropped to nearly 20 samples per second. Using laser sheet lighting for flow visualization purposes, seed

particles near the vortex core were observed to centrifuge outwards radially. To avoid these flow tracking problems, the mineral oil used for flow field seeding was size discriminated prior to injection into the wind tunnel. Based on the results of Dring and Suo (ref. 5), the Stokes flow model showed that a 1 micron diameter particle subjected to a radial acceleration of 150,000 meters per second squared (500 fps at a 1 in radius) resulted in a Stokes number of approximately 0.01. The tracking error associated with this situation is estimated at 3% in angular deviation. This analysis, as depicted in figure 17, warranted the use of a particle impactor to maintain seed size distribution centerlines below 1 micron in diameter.

Results of the 3-D LV surveys are shown in figures 18a-18f. These crossflow velocity vector plots show the chordwise development of the leading edge vortex at an angle of attack of 10 degrees. An examination of figures 18a and 18b shows only a single center or vorticity, apparently because the circumferential pressure gradient causes a coalescence of separate vortices from the strake and the wing leading edge. Contrasting these results, surveys taken at 18 degrees angle of attack showed vortex breakdown near the mid-chord location. Axial velocities, as shown in figure 19, change dramatically at vortex breakdown. The high peak in this velocity at 25% chord is entirely absent at 50% chord. Note that for the 18 degree angle of attack case, reversed axial velocities are seen near the center of the vortex. This can be directly attributed to a breakdown of the organized vortical flow. Lastly, as a result of the various surveys, the vortex core location can be tracked as a function of chord, span and height above the wing reference plane. Vortex breakdown and path are shown in figure 20 for both the 10 degree and 18 degree angle-of-attack cases.

RECOMMENDATIONS AND CONCLUSIONS

The 2 x 2-D LV method described was demonstrated to be a very powerful tool in making 3-D flow field measurement. The 3-D data were shown to be obtainable using a conventional 2-D instrument; however, due to its inaccuracies, it is recommended that its use should be carefully applied to particular situations that require turbulence information in addition to mean velocities. In the design study of two fully three-dimensional LV's, the three-color system was shown to be superior overall in both range and resolution. For these reasons, the system was fabricated for use in production testing of highly three-dimensional and vortical flows. Measurements over a generic fighter flow field justify the use of two large Argon-ion lasers. Based on this experience, it is recommended that higher powered lasers (0.5-1.0 watts/ beam) be used to offset the diminished signal-to-noise ratios that are found at or near the core of a vortex.

REFERENCES

1. Yeh, Y. and Cummins, H. Z., "Localized Fluid Flow Measurements with a He-Ne Laser Spectrometer," Applied Physics Letter, Vol. 4, 1964, p. 176.

2. Yanta, W. J. "The Use of the Laser Doppler Velocimeter in Aerodynamic Facilities," AIAA 11th Aerodynamic Testing Conference, AIAA Paper 80-0435, March 18-20, 1980.

3. Orloff, K. L. and Snyder, P. K., "Reduction of Flow-Measurement Uncertainties in Laser Velocimeters with Nonorthogonal Channels," AIAA 21st Aerospace Sciences Meeting, AIAA Paper 83-0051, January 10-13, 1983, Reno, NV.

4. Yanta, W. J., "A Three-Dimensional Laser Doppler Velocimeter (LDV) for use in Wind Tunnels," ICIASF '79 Record, September 1979, Monterey, California.

5. Dring, R. P. and Suo, M., "Particle Trajectories in Swirling Flows," J. Energy, Vol. 2, No. 4, July-August 1978.

GAW-1W/LV Mean Velocity Profiles

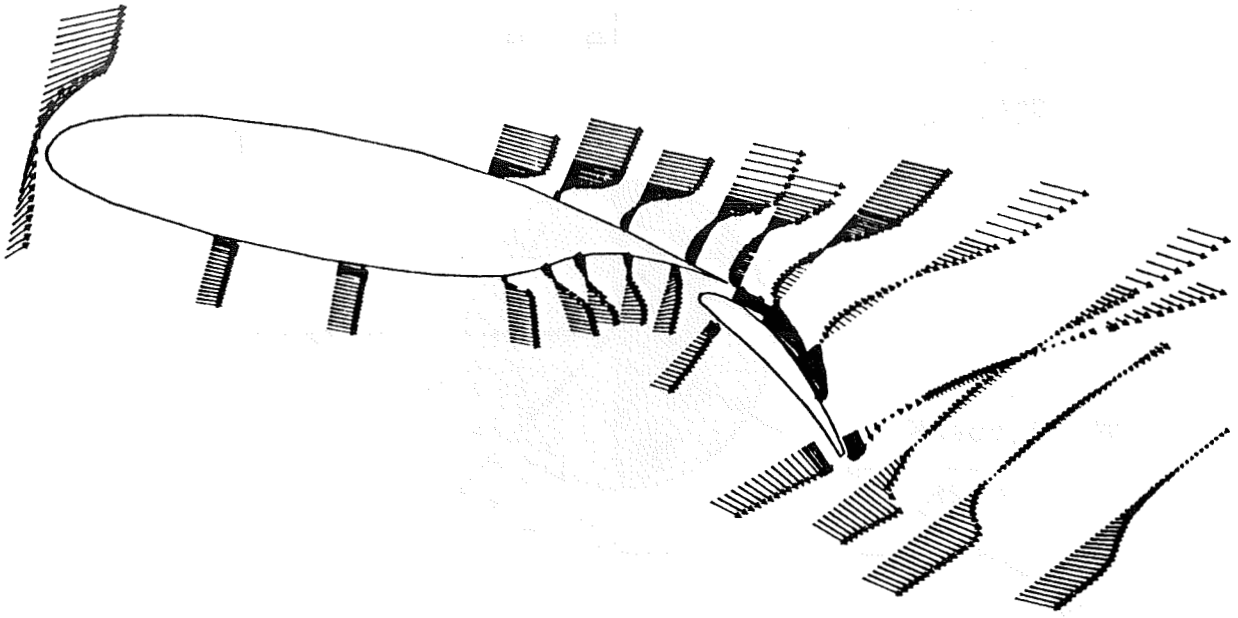

Figure 1

CCW/LV Mean Velocity Vectors

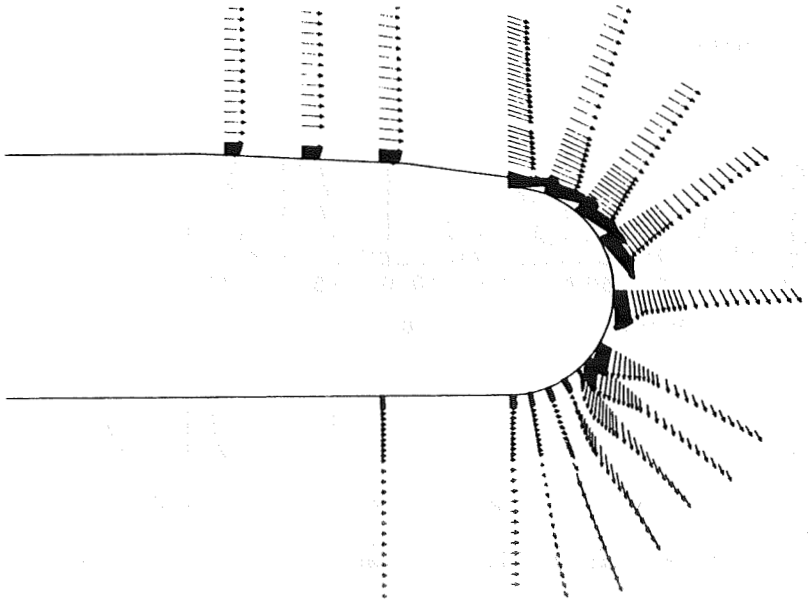

Figure 2

LV Fringe and Wind Tunnel Coordinate System

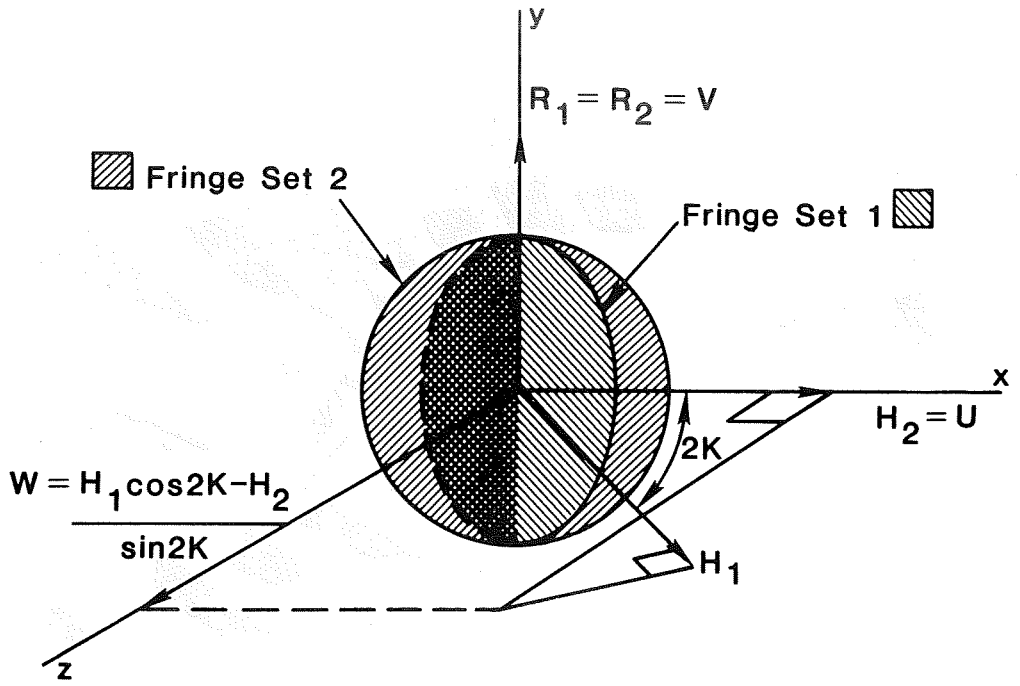

Figure 3

3-D Boundary Layer Measurements Using 2x2D Method

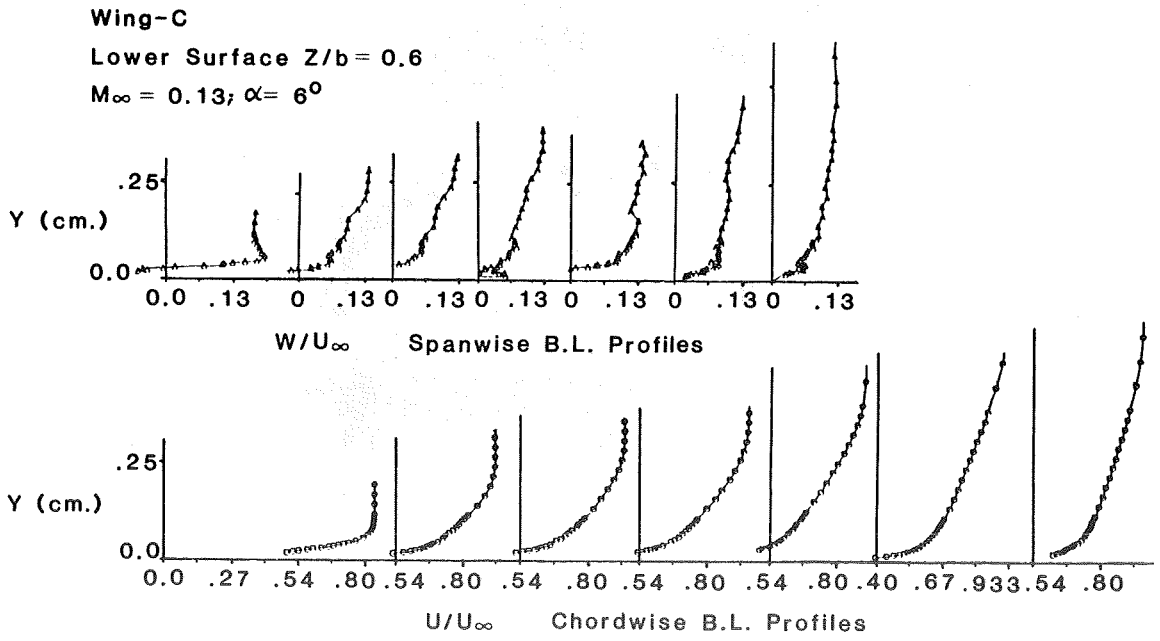

Figure 4

Turbulence Anisotropy Measurements Using 2X2D Method

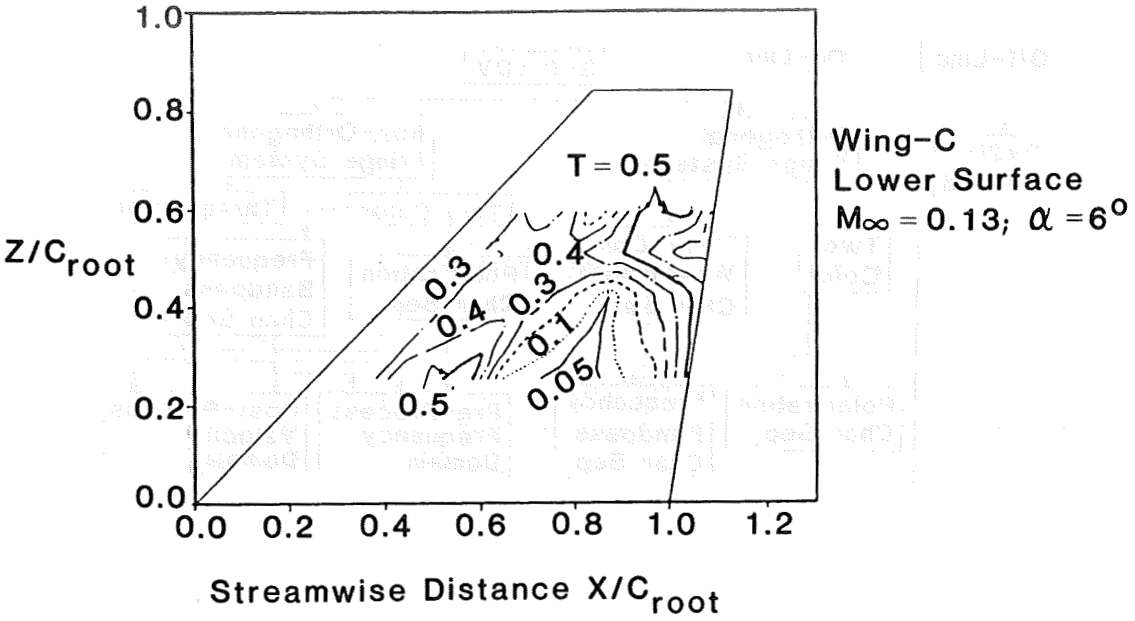

Figure 5

Aft-Fuselage Measurements Using 2x2D Method

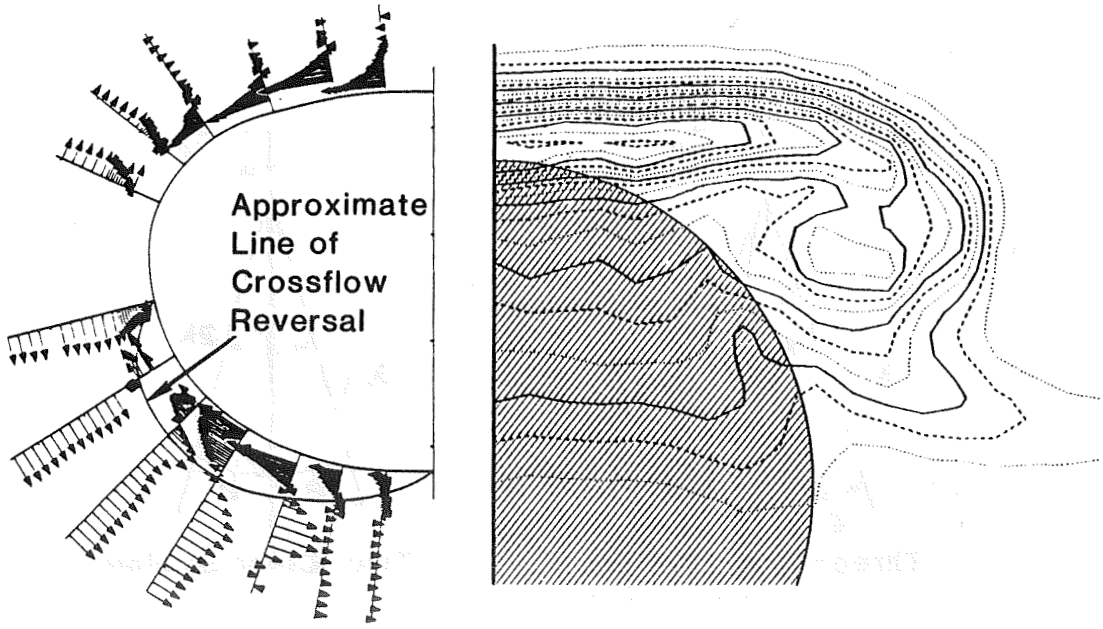

a) Crossflow Boundary Layers b) Near Wake Axial Velocity

Figure 6

3-D LV Optical Configurations

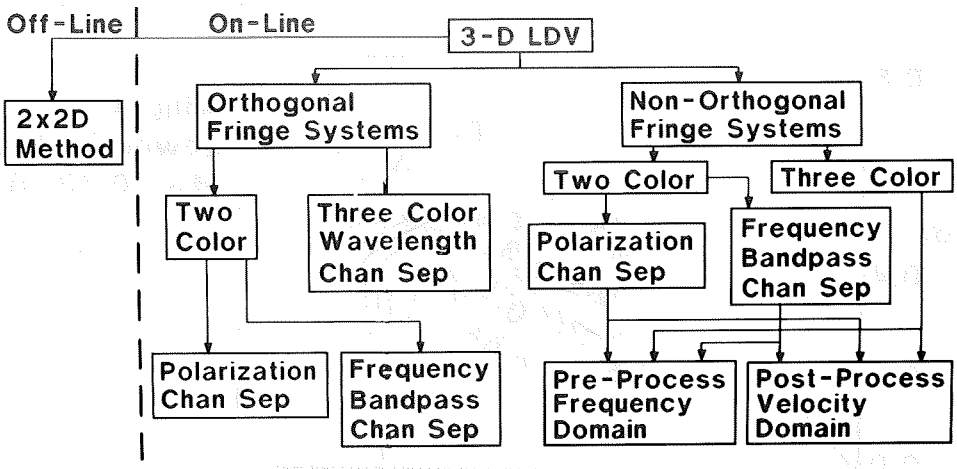

Figure 7

3-D LV Optical Beam Traces

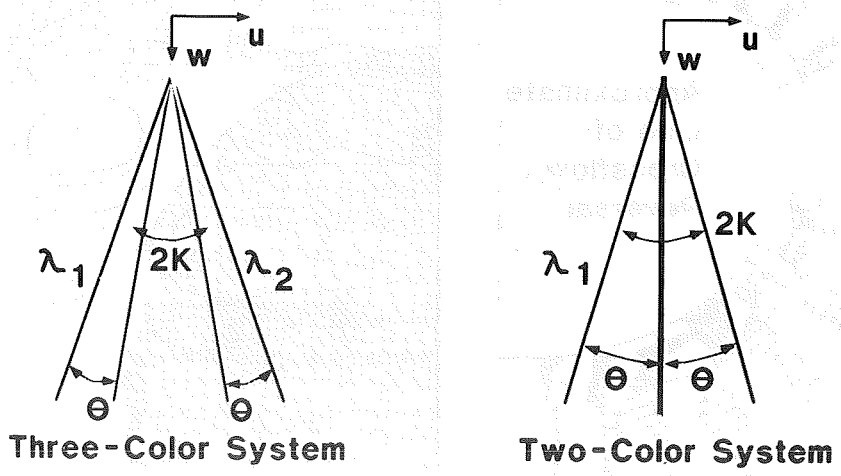

Figure 8

Formation of Effective Fringes

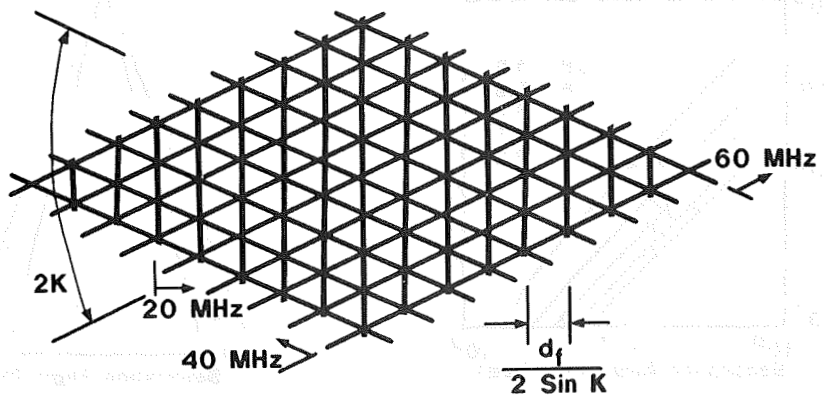

Figure 9

Double Balanced RF Mixer

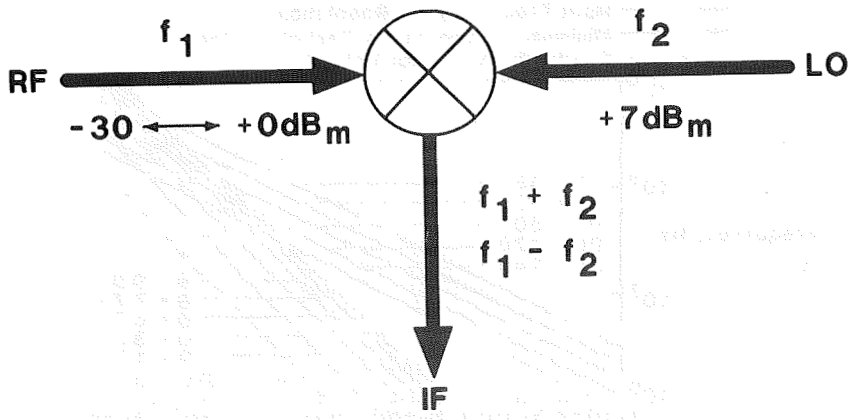

Figure 10

Effective Fringe Spacing vs. Separation Angle

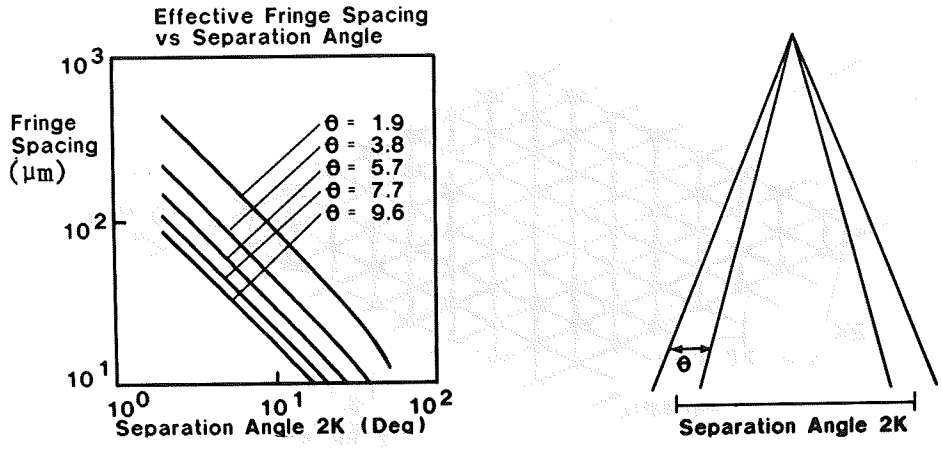

Figure 11

Velocity Range and Resolution Chart for 3-D LV Design

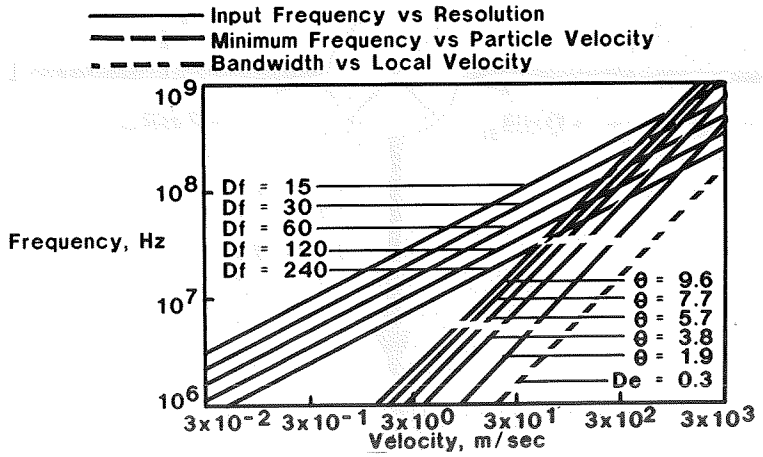

Figure 12

3-D LV Frequency Domain Processing Circuits

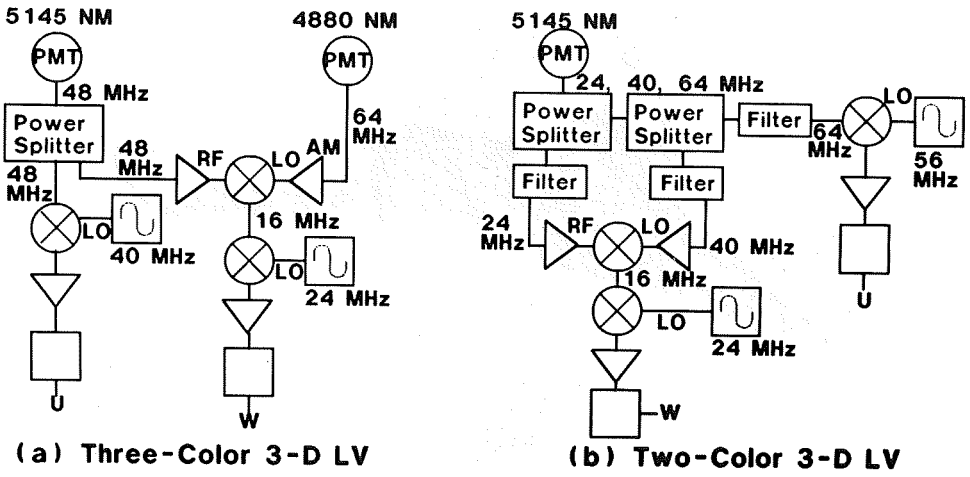

Figure 13

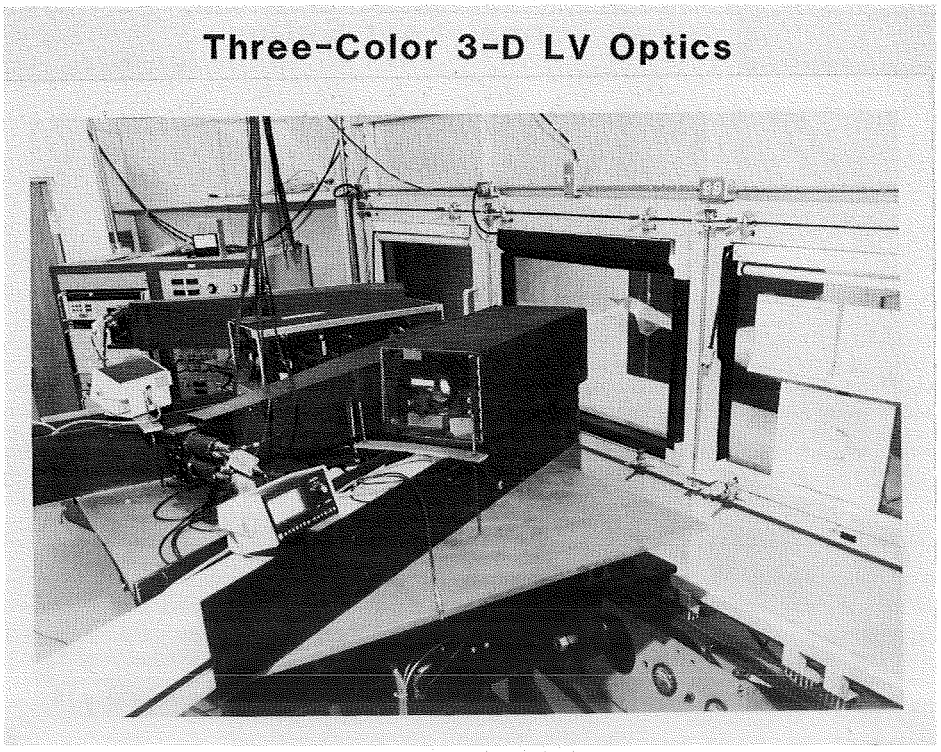

Figure 14

Generic Fighter Configuration

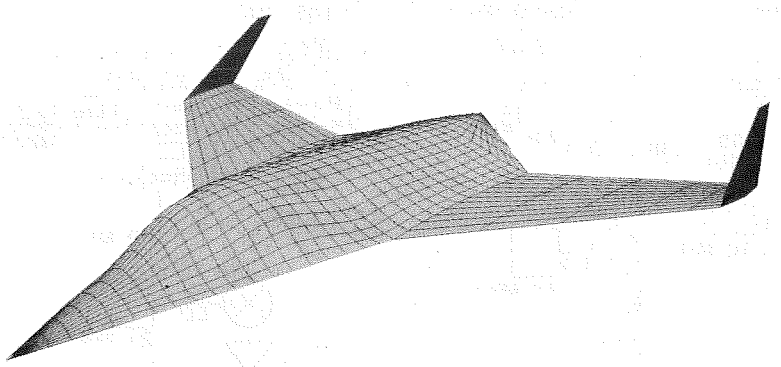

Figure 15

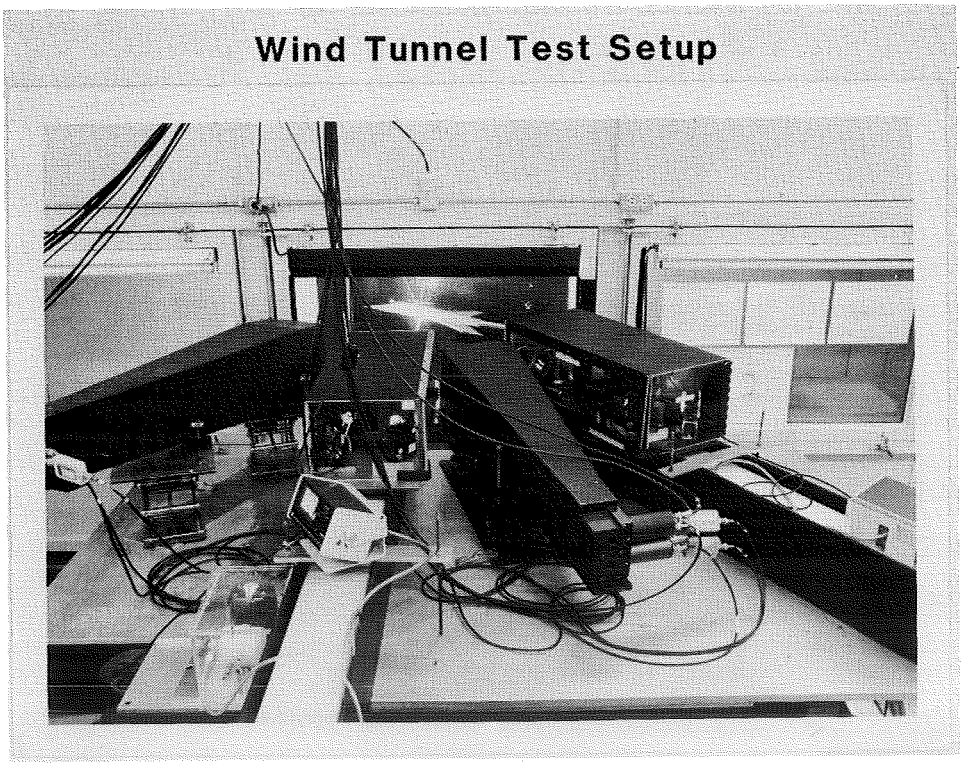

Figure 16

Seed Particle Behavior in a Vortical Flow

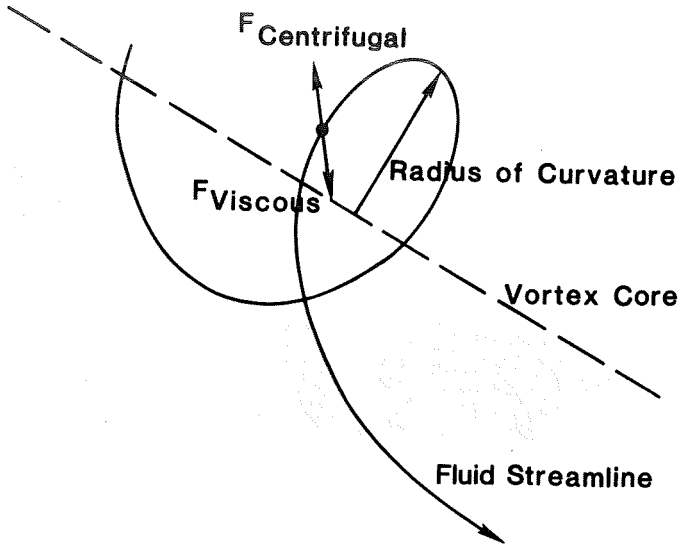

Figure 17

Mean Crossflow Velocity Vectors

$\alpha = 10^{o}$ $x/c = 0.000$

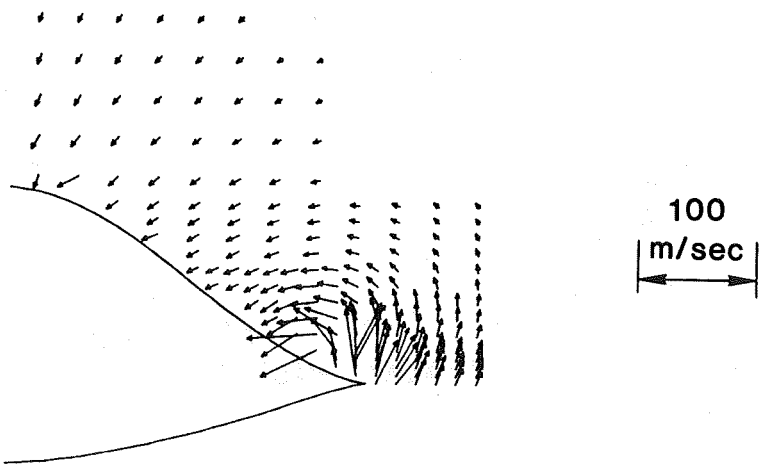

(a)

Figure 18

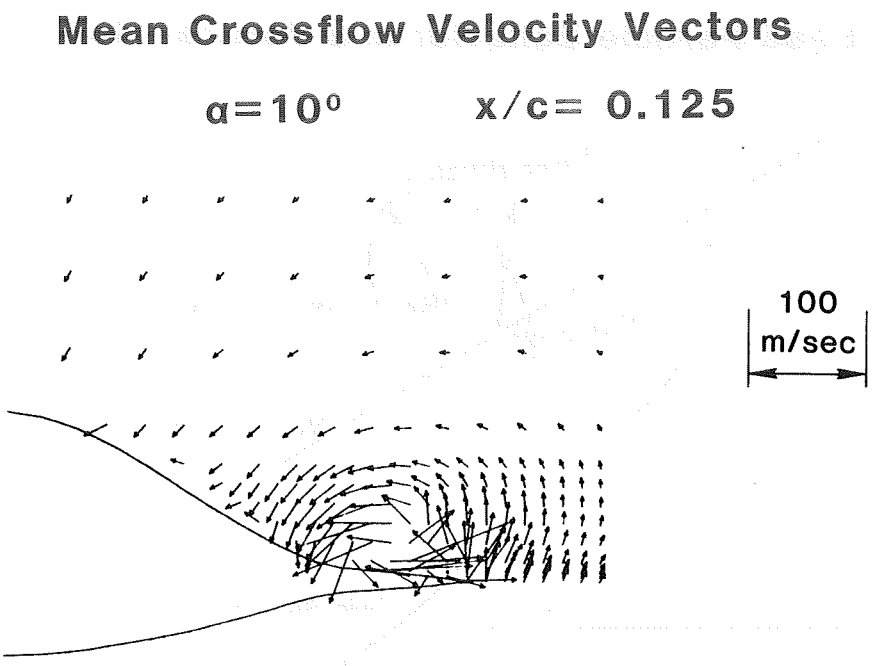

(b)

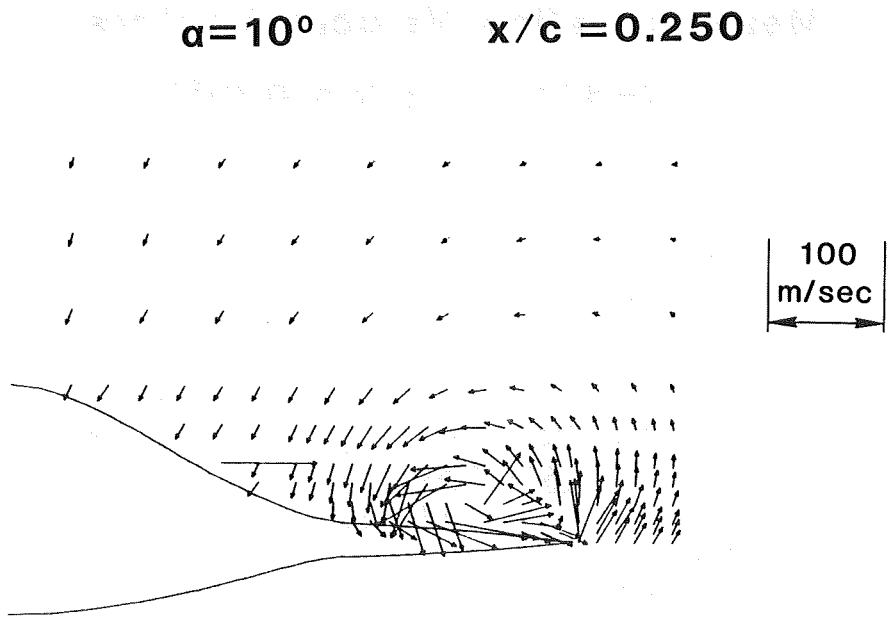

(c)

Figure 18 (Continued)

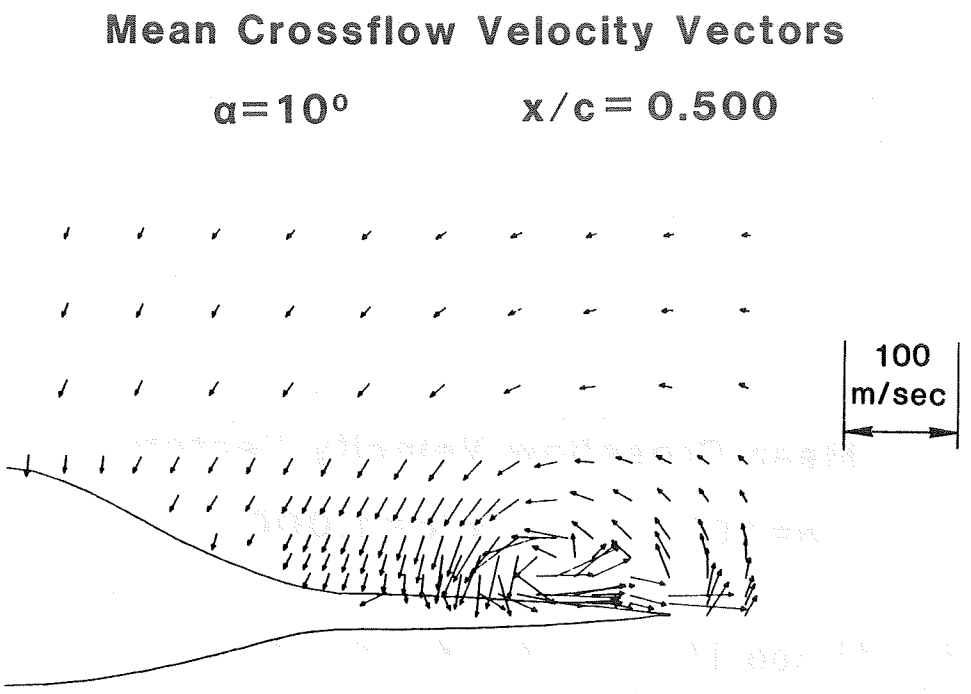

(d)

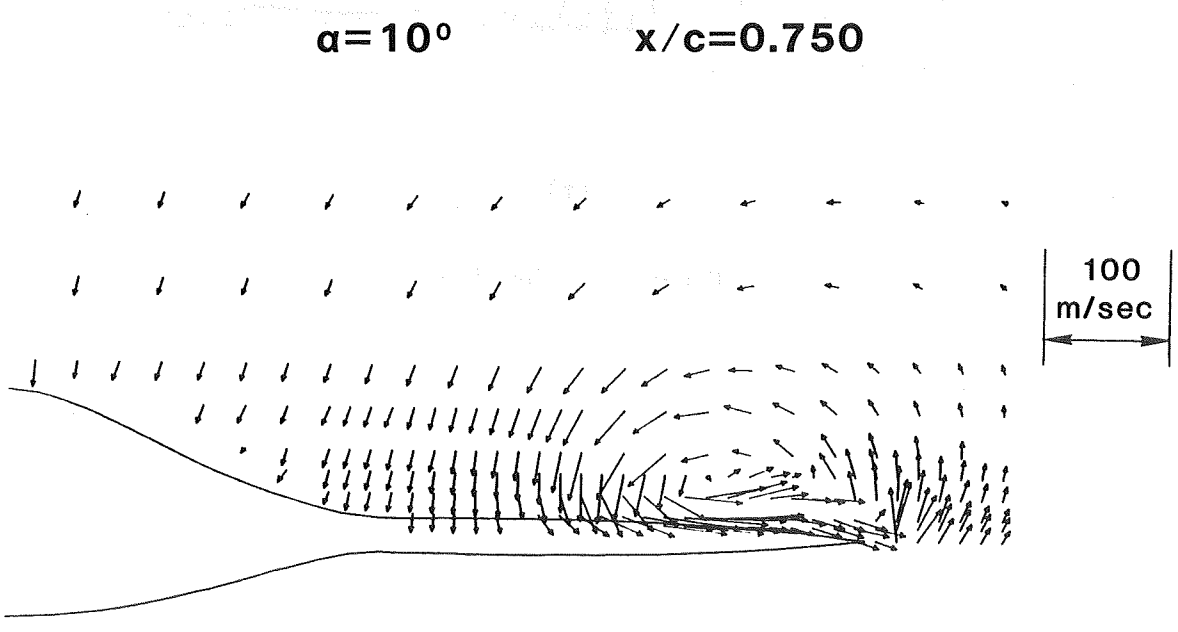

(e)

Figure 18 (Continued)

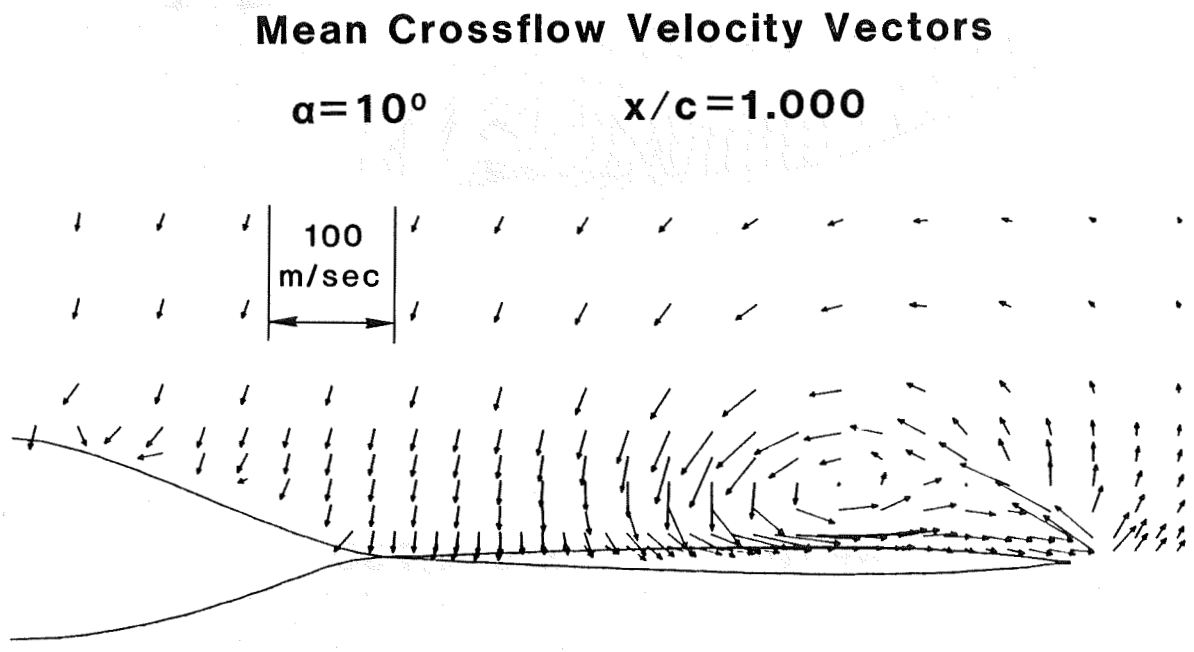

(f)

Figure 18 (Concluded)

C-23

Vortex Track

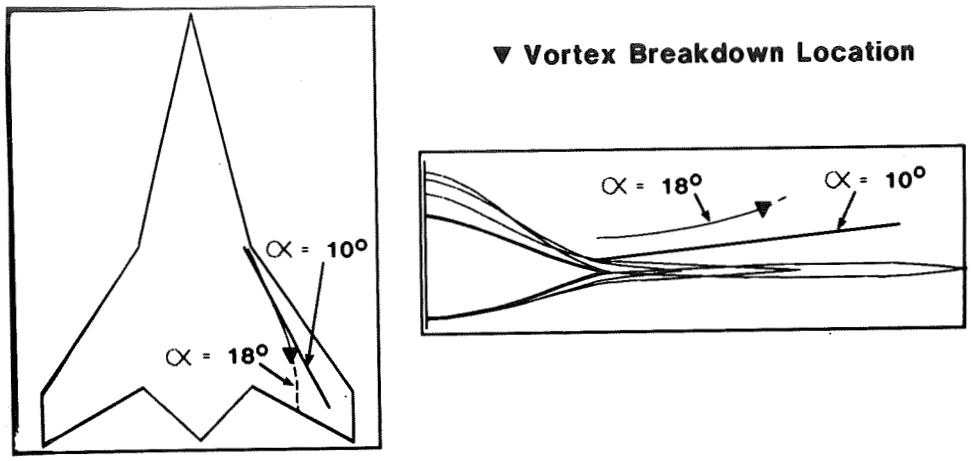

Figure 19

Mean Axial Velocity

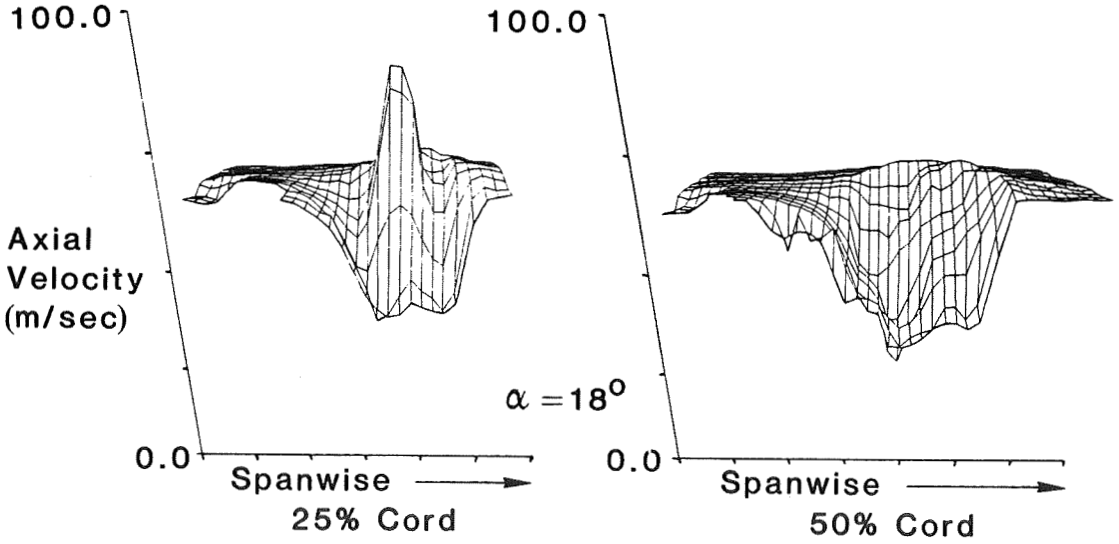

Figure 20